Particle-based model for skiing traffic

Thomas Holleczek[*] and Gerhard Tröster[†]
Wearable Computing Lab, ETH Zurich, Gloriastrasse 35, CH-8092 Zurich, Switzerland
(Received 9 December 2011; revised manuscript received 5 March 2012; published 3 May 2012)

We develop and investigate a particle-based model for ski slope traffic. Skiers are modeled as particles with a mass that are exposed to social and physical forces, which define the riding behavior of skiers during their descents on ski slopes. We also report position and speed data of 21 skiers recorded with GPS-equipped cell phones on two ski slopes. A comparison of these data with the trajectories resulting from computer simulations of our model shows a good correspondence. A study of the relationship among the density, speed, and flow of skiers reveals that congestion does not occur even with arrival rates of skiers exceeding the maximum ski lift capacity. In a sensitivity analysis, we identify the kinetic friction coefficient of skis on snow, the skier mass, the range of repelling social forces, and the arrival rate of skiers as the crucial parameters influencing the simulation results. Our model allows for the prediction of speed zones and skier densities on ski slopes, which is important in the prevention of skiing accidents.

DOI: 10.1103/PhysRevE.85.056101 PACS number(s): 89.65.−s, 89.40.−a, 45.70.Vn

I. INTRODUCTION

Modeling traffic has attracted the interest of physicists in recent decades and has a major impact on everyday life [1]. These models can, for instance, illustrate the one-dimensional traffic of vehicles [2–11] in order to study the formation of congestion and its properties. In two dimensions, the traffic of pedestrians is investigated [12–19] in order to predict pedestrian flows in normal as well as panic situations and emergencies. In the case of three-dimensional traffic, the flocking of birds [20] and the formation of fish schools [21] are studied. The methods to model these scenarios range from macroscopic (fluid-dynamic) [3,9] to mesoscopic (gas-kinetic) [22] and microscopic (particle-based) [2,14] approaches, as well as lattice gas automata [4,5]. They can further be divided into many-particle systems, in which particles are driven by external forces such as gravity or friction, and self-driven many-particle systems, where the driving force is self-produced [23].

Although common systems such as vehicular traffic and the behavior of pedestrians have already been investigated thoroughly, the field of traffic in sports remains largely unexplored. We base our model in a snow-sport environment due to the fact that skiing is among the fastest-growing sports in the world, attracting an estimated 10 million active participants solely in the United States [24]. However, accidents as well as fatalities happen frequently [25–29]. According to a safety study of the National Ski Areas Association, there are 150,000 accidents on U.S. ski slopes every year, roughly 39 of which end fatally [30]. The majority of the reported incidents occur when skiers and snowboarders descend the trails too rapidly, overestimating their skills. In many cases, collisions of the participants are involved, especially at intersections of ski slopes and when the density of skiers is high [31].

In this article, we aim at establishing a theoretical framework for the modeling of skiing traffic and its validation with experiments. Our model can be classified as a two-dimensional microscopic-driven many-particle system with the natural constraint that motion usually occurs in the trail downhill direction and skiers are exposed to gravity and centripetal forces. We cover the properties of the forces acting on skiers and determine interactions between them. Moreover, we put our model to the test with the help of the motion data on 21 skiers recorded on two Swiss ski slopes with GPS-equipped cell phones. Finally, we show that our model allows for the prediction of areas on ski slopes that are prone to high speeds and skier density, which are both factors favoring the occurrence of accidents [30,31]. Thus, it is likely to be advantageous in the prevention of accidents—as is the case for pedestrian models [32].

In particular, Sec. II summarizes our approach to modeling ski slope traffic. Section III reports the results of position and speed measurements we conducted on two Swiss ski slopes. Section IV presents the major results obtained by computer simulations of the model. Moreover, it evaluates the model by comparing the simulated with the measured speed. Section V reports the effect of varying the model input parameters on the simulation results in a sensitivity analysis. We conclude our work in Sec. VI.

II. MODEL

This section presents our approach to modeling ski slope traffic. In particular, Sec. II A introduces the principles of skiing. Section II B gives an overview of our model. Section II C introduces the concept of social forces for skiers as a basis for directional choices and Sec. II D analyzes the physical forces skiers are exposed to.

A. Skiing basics

The principle of skiing is to slide down snow-covered slopes on skis by manipulating gravity and performing turns across the fall line. Snow-sport athletes want to reach a final destination, namely, the end of the ski slope. Normally, they do not choose the fastest route per definition: by performing turns across the fall line, snow-sport athletes can control their direction of motion and speed.

[*]hollthom@ethz.ch
[†]troester@ife.ee.ethz.ch

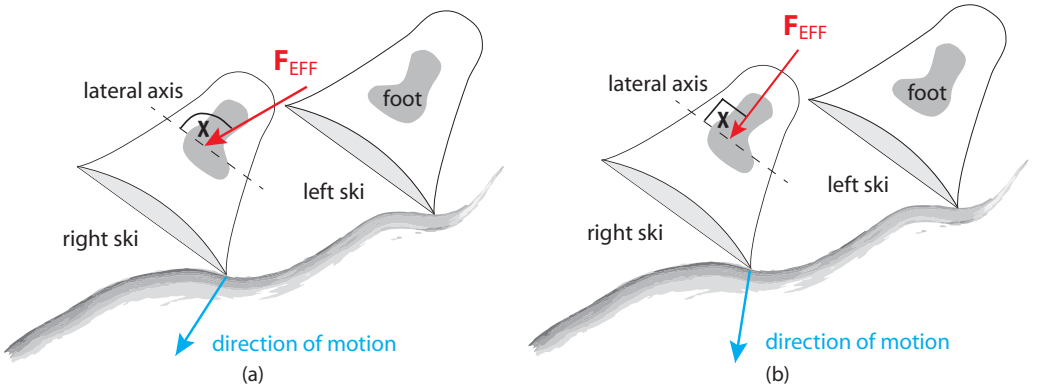

FIG. 1. (Color online) Skidded (a) and carved (b) turns from the frontal perspective. (a) During skidded turns, the angle χ between the skier's effective force $\mathbf{F}_{\mathrm{EFF}}$ and the lateral axis of the skis is greater than 90°. Therefore, the skis also slip away to the side. (b) During carved turns, the effective force $\mathbf{F}_{\mathrm{EFF}}$ is perpendicular to the lateral axis of the skis ($\chi = 90°$). The direction of motion is exclusively parallel to the skis.

There are two major techniques of performing turns: *skidding* and *carving* (see Fig. 1). During skidded turns, the motion direction is parallel to the skis. However, it includes an additional slippage to the side, which is displayed in Fig. 1(a). In contrast to skidding, the direction of motion is exclusively parallel to the skis during carved turns. Skiers have to make sure the pressure applied to a ski, which we refer to as his or her *effective force* $\mathbf{F}_{\mathrm{EFF}}$, is perpendicular to the lateral axis of the ski [see Fig. 1(b)]. Skidding is a technique normally used by beginners at skiing, whereas carving is more difficult to learn and considered to be the most elegant way of skiing.

Studies have shown that skiers perform turns with a radius corresponding to the so-called *sidecut radius* R_{sc} of their skis [33,34]. The sidecut radius is also known as the *curvature radius* and is an intrinsic property of carving skis (see Fig. 2).

Naturally, snow-sport athletes can only follow the downhill direction imposed by the slope and do not go backward. To avoid dangerous collisions, they try to keep away from other skiers and obstacles on the slope. Moreover, slope operators do not usually permit off-piste skiing for safety reasons (avalanches, hidden rocks, etc.) and require all participants to stay on the trail. Therefore, snow-sport athletes also try to keep away from the edges of the slope during their descents. Finally, skiers cannot always perceive all situations on the slope, for example, when the view is limited due to fog or snow storms, which can lead to accidents such as collisions.

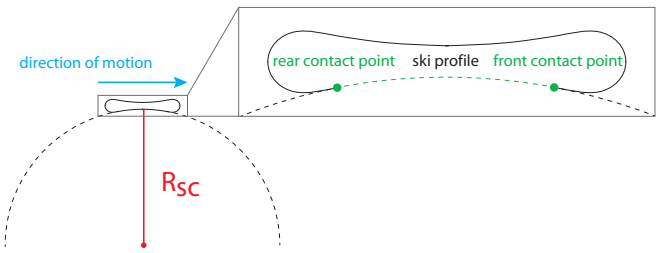

FIG. 2. (Color online) Profile of a modern carving ski. The sidecut radius R_{sc} is an an intrinsic property of carving skis. It corresponds to the size of the turn the skis will make when set on edge. The sidecuts of modern carving skis are designed for a turn radius ranging from 7 to 15 m [35].

B. Skiing model

We model the riding behavior of snow-sport athletes described above with a two-dimensional microscopic-driven many-particle system. Snow-sport athletes are modeled as particles with mass m. The vector $\mathbf{r}(t)$ denotes the position of a particular skier; $\dot{\mathbf{r}}(t) = \frac{\mathrm{d}}{\mathrm{d}t}\mathbf{r}(t)$, his or her speed; and $\mathbf{e}_{\dot{\mathbf{r}}}(t) = \dot{\mathbf{r}}(t)/\|\dot{\mathbf{r}}(t)\|$, his or her direction of motion at time t. There are two types of forces that define the trajectories of a skier riding downhill.

(1) Lewin [36] introduced so-called *social forces* to model human behavior. We use these social forces to attract skiers toward waypoints they want to reach, repel them from edges of the slope, and prevent them from colliding with other participants or obstacles (see Sec. II C). The superposition $\mathbf{F}_{\mathrm{social}}$ of all social forces that a skier is exposed to indicates his or her desired direction of motion as $\mathbf{e}_{\mathrm{social}} = \mathbf{F}_{\mathrm{social}}/\|\mathbf{F}_{\mathrm{social}}\|$. Should the angle between the desired direction $\mathbf{e}_{\mathrm{social}}$ and the current direction of motion $\mathbf{e}_{\dot{\mathbf{r}}}$ exceed a predefined threshold angle δ (i.e., if $\mathbf{e}_{\dot{\mathbf{r}}} \cdot \mathbf{e}_{\mathrm{social}} \leqslant \cos\delta$), the skier adjusts his or her direction by performing a turn toward the desired direction. Otherwise, the skier maintains the direction of motion (see Fig. 3).

(2) We also consider the *physical forces* acting in this scenario (see Sec. II D). The gravitational, centripetal, and

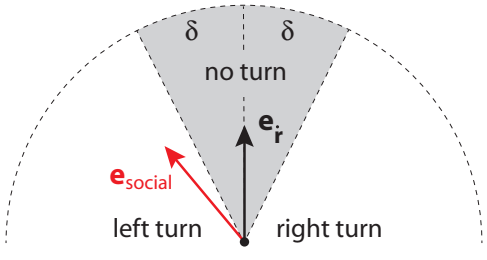

FIG. 3. (Color online) Should the angle between the desired direction $\mathbf{e}_{\mathrm{social}}$ and the current direction of motion $\mathbf{e}_{\dot{\mathbf{r}}}$ exceed the threshold angle δ, the skier adjusts his or her direction by performing a corresponding turn from $\mathbf{e}_{\dot{\mathbf{r}}}$ to $\mathbf{e}_{\mathrm{social}}$. Otherwise, the skier maintains the current direction of motion. In the case illustrated here, the angle between $\mathbf{e}_{\mathrm{social}}$ and $\mathbf{e}_{\dot{\mathbf{r}}}$ is greater than δ, and the skier will turn left.

friction forces accelerate and decelerate the skier according to his or her desired direction $\mathbf{e}_{\text{social}}$.

Often, ski slopes feature counter slopes, i.e., areas where skiers have to ride uphill rather than downhill. These counter slopes slow skiers down and can even force them to walk. Our model also deals with this case: should skiers come to a complete halt due to a counter slope, they will start walking uphill at a constant speed until they have passed it successfully.

Our model has the following limitations: we have only included skiers and ignore other snow-sport athletes such as snowboarders and Telemark skiers. Moreover, skiers are not allowed to jump or ever to stop during their descents. They ride independently and do not form into groups. Although usually prohibited, skiers sometimes pass the edges of the slope for the fresh and unprepared snow off-piste. In our model, we assume that skiers are not allowed to leave a slope. Should skiers collide with either slope edge during their descent, they will be reflected back to the corresponding center point of the slope. Finally, we only consider skiers performing carved turns with the sidecut radius R_{sc} and ignore skidded turns or varying radii. By comparing the real and the simulated position and speed data of skiers, we show that our model is—despite these limitations—capable of describing skiing traffic well (see Sec. IV).

C. Social forces

The concept of social forces was first presented by Lewin [36] to model human behavior; it was later put into mathematical terms by Helbing [37] and used in a particle-based model for pedestrian dynamics [14]. Analogously, we introduce social forces to model the behavior of skiers. Unlike in pedestrian models, however, the superposition of all social forces, which we refer to as $\mathbf{F}_{\text{social}}$, does not accelerate a skier physically: we define the net social force $\mathbf{F}_{\text{social}}$ as dimensionless. Its direction $\mathbf{e}_{\text{social}} = \mathbf{F}_{\text{social}}/\|\mathbf{F}_{\text{social}}\|$ decides whether skiers need to adjust their current direction of motion $\mathbf{e}_{\dot{\mathbf{r}}}$ by performing a corresponding turn (see Fig. 3).

In our model, we assume that every skier a selects several consecutive waypoints $\mathbf{x}_a^1, \ldots, \mathbf{x}_a^n$ on the slope he or she desires to reach. Let $\mathbf{x}_a^k$ denote the next desired waypoint. The direction toward the next waypoint can then be expressed as

$$\mathbf{e}_a(t) = \frac{\mathbf{x}_a^k - \mathbf{r}_a(t)}{\left\|\mathbf{x}_a^k - \mathbf{r}_a(t)\right\|}, \tag{1}$$

where $\mathbf{r}_a(t)$ is the current position of a on the slope at time t. We introduce the *destination force* $\mathbf{F}_D$, which guides skier a toward the next desired waypoint $\mathbf{x}_a^k$, as

$$\mathbf{F}_D(\mathbf{r}_a) = A_0 \mathbf{e}_a(t), \tag{2}$$

where A_0 is a dimensionless scaling constant, which models the strength of the desire of the skier to move in a certain direction, and $\mathbf{e}_a(t)$ is the direction toward the next waypoint according to Eq. (1).

Intuitively, most skiers try to keep away from the left and right edge of the slope they are descending to decrease the risk of accidents. Apparently, the closer a skier is to an edge, the stronger the repulsive effect will be. We model this observation with the help of a social force we refer to as *edge repulsion*. Let $\mathbf{r}_{aL}$ be the distance of skier a from the left edge of the slope. It can be written as $\mathbf{r}_{aL} = \mathbf{r}_a - \mathbf{r}_a^L$, where $\mathbf{r}_a^L$ represents the location on the left slope edge closest to the current position of the skier. We define the force repelling the skier from the left slope edge $\mathbf{f}_L$ with the help of a monotonically decreasing potential $U(\|\mathbf{r}_{aL}\|)$ as

$$\mathbf{f}_L(\mathbf{r}_{aL}) = -\nabla_{\mathbf{r}_{aL}} U(\|\mathbf{r}_{aL}\|). \tag{3}$$

The force $\mathbf{f}_R$ repelling the skier from the right slope edge can be defined analogously.

The directional choice of an athlete a is also influenced by other athletes on the slope. Intuitively, a will try to keep away from them to avoid dangerous collisions. We account for this fact with the introduction of the *athlete repulsion* $\mathbf{f}_A$ another skier b imposes on a as

$$\mathbf{f}_A(\mathbf{r}_{ab}) = -\nabla_{\mathbf{r}_{ab}} V[s(\mathbf{r}_{ab})]. \tag{4}$$

As introduced by Helbing [14], we assume that $V_{ab}(s)$ is a monotonically decreasing potential with equipotential lines that have the form of an ellipse directed into the direction of motion. Here, s represents the semiminor axis of this ellipse:

$$s(\mathbf{r}_{ab}) = \frac{\sqrt{(\|\mathbf{r}_{ab}\| + \|\mathbf{r}_{ab} - v_b\,\Delta\tau\,\mathbf{e}_b\|)^2 - (v_b\,\Delta\tau)^2}}{2}, \tag{5}$$

where $\mathbf{r}_{ab} = \mathbf{r}_a - \mathbf{r}_b$, $v_b = \|\dot{\mathbf{r}}_b\|$ is the speed of b and $\mathbf{e}_b$ is the direction toward b's next waypoint.

We also take into account obstacles on the ski slope such as snow guns or piles of ski lifts, which skiers try to ride around. The repulsive effect will be stronger the closer a skier approaches an obstacle. We introduce the *obstacle repulsion* $\mathbf{f}_O$ an obstacle o imposes on skier a as

$$\mathbf{f}_O(\mathbf{r}_{ao}) = -\nabla_{\mathbf{r}_{ao}} W(\|\mathbf{r}_{ao}\|), \tag{6}$$

where $\mathbf{r}_{ao} = \mathbf{r}_a - \mathbf{x}_o$. $\mathbf{x}_o$ denotes the position of obstacle o on the slope, and we define $W(\|\mathbf{r}_{ao}\|)$ as a monotonically decreasing potential.

So far, we have assumed that skiers are capable of perceiving objects they are repelled by at any distance. However, the view on ski slopes might be limited due to fog or snow. To take this into account, we introduce the weight

$$u(\mathbf{r},d) = \begin{cases} 1 & \text{if} \|\mathbf{r}\| \leqslant d, \\ 0 & \text{otherwise}, \end{cases} \tag{7}$$

where d is the current visibility on the slope. Multiplied by the repelling forces, this weight makes sure that skiers cannot see any objects farther away than distance d. Moreover, skiers may only perceive objects within a certain range of their current direction of motion, which we refer to as the *angle of view* 2φ, which we model with the weight

$$w(\mathbf{u},\mathbf{v}) = \begin{cases} 1 & \text{if}(\mathbf{u}/\|\mathbf{u}\|) \cdot (\mathbf{v}/\|\mathbf{v}\|) \geqslant \cos\varphi, \\ 0 & \text{otherwise}. \end{cases} \tag{8}$$

By taking into account the presented weights for visibility and angle of view multiplicatively, we obtain the resulting repelling social forces as

$$\mathbf{F}_L(\dot{\mathbf{r}}_a,\mathbf{r}_{aL}) = u(\mathbf{r}_{aL},d)w(\dot{\mathbf{r}}_a, -\mathbf{r}_{aL})\mathbf{f}_L(\mathbf{r}_{aL}), \tag{9}$$

$$\mathbf{F}_R(\dot{\mathbf{r}}_a,\mathbf{r}_{aR}) = u(\mathbf{r}_{aR},d)w(\dot{\mathbf{r}}_a, -\mathbf{r}_{aR})\mathbf{f}_R(\mathbf{r}_{aR}), \tag{10}$$

$$\mathbf{F}_A(\dot{\mathbf{r}}_a,\mathbf{r}_{ab}) = u(\mathbf{r}_{ab},d)w(\dot{\mathbf{r}}_a, -\mathbf{r}_{ab})\mathbf{f}_A(\mathbf{r}_{ab}), \tag{11}$$

$$\mathbf{F}_O(\dot{\mathbf{r}}_a,\mathbf{r}_{ao}) = u(\mathbf{r}_{ao},d)w(\dot{\mathbf{r}}_a, -\mathbf{r}_{ao})\mathbf{f}_O(\mathbf{r}_{ao}). \tag{12}$$

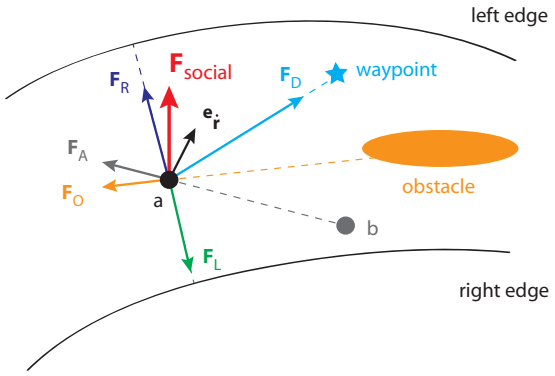

FIG. 4. (Color online) Illustration of social forces. The slope is shown in top view. $\mathbf{F}_D$ attracts skier a toward the next waypoint. The forces $\mathbf{F}_L$ and $\mathbf{F}_R$ repel a from the left and right edge of the slope, respectively. $\mathbf{F}_A$ keeps a away from other skiers, and $\mathbf{F}_O$ repels a from obstacles.

Finally, the net social force $\mathbf{F}^a_{\text{social}}$ acting on skier a can be determined as the superposition of all weighted social forces as

$$\mathbf{F}^a_{\text{social}} = \mathbf{F}_D(\mathbf{r}_a) + \mathbf{F}_L(\dot{\mathbf{r}}_a, \mathbf{r}_{aL}) + \mathbf{F}_R(\dot{\mathbf{r}}_a, \mathbf{r}_{aR}) + \sum_b \mathbf{F}_A(\dot{\mathbf{r}}_a, \mathbf{r}_{ab}) + \sum_o \mathbf{F}_O(\dot{\mathbf{r}}_a, \mathbf{r}_{ao}). \quad (13)$$

The direction $\mathbf{e}_{\text{social}} = \mathbf{F}_{\text{social}}/\|\mathbf{F}_{\text{social}}\|$ of the net social force indicates where an snow-sport athlete a wants to travel and decides whether an adjustment of the current direction of motion $\mathbf{e}_{\dot{\mathbf{r}}}$ through a corresponding turn is necessary (see Fig. 3). Figure 4 illustrates the social forces acting on a skier.

D. Physical forces

In this section, we derive the major physical forces skiers are exposed to. Lind [38] and Jentschura [34] have presented an overview of forces occurring during skiing. Let us consider a skier at position $\mathbf{r}$ with the speed vector $\dot{\mathbf{r}}$, the direction of motion $\mathbf{e}_{\dot{\mathbf{r}}}$, and mass m. Moreover, let $\mathbf{n}$ denote the surface normal on the slope at $\mathbf{r}$. Then the slope has an inclination of

$$\alpha = \arccos([0,0,1]^T \cdot \mathbf{n}) \quad (14)$$

at $\mathbf{r}$. Moreover, let $\beta \in [0^\circ, 180^\circ]$ denote the angle between the current trajectory $\mathbf{e}_{\dot{\mathbf{r}}}$ of the skier and the horizontal of the slope at $\mathbf{r}$. Then the inclination angle γ of $\mathbf{e}_{\dot{\mathbf{r}}}$ is

$$\gamma = \arcsin[(\sin\alpha)(\sin\beta)]. \quad (15)$$

Let us now investigate the various physical forces. First, skier a is exposed to the *gravitational force* $\mathbf{F}_G$

$$\mathbf{F}_G = mg \begin{bmatrix} 0 \\ 0 \\ -1 \end{bmatrix}, \quad (16)$$

where g represents the gravitational acceleration of the Earth and m the mass of the skier. The *normal force* $\mathbf{F}_N$ acting on the skier is parallel to the surface normal $\mathbf{n}$ at $\mathbf{r}$ and can be written as

$$\mathbf{F}_N = mg(\cos\alpha)\mathbf{n}. \quad (17)$$

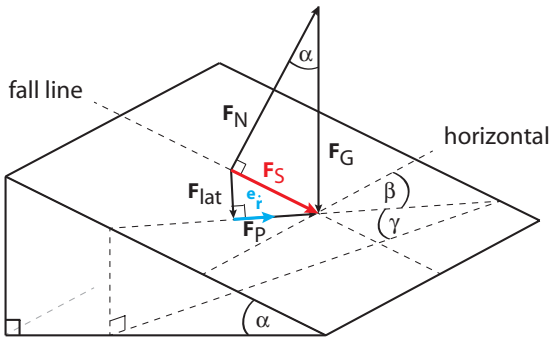

FIG. 5. (Color online) The downhill force $\mathbf{F}_S$ parallel to the fall line can be decomposed into a lateral force $\mathbf{F}_{\text{lat}}$ and a downhill force $\mathbf{F}_P$ accelerating the skier along $\mathbf{e}_{\dot{\mathbf{r}}}$.

As illustrated in Fig. 5, the *downhill force* acting parallel to the fall line $\mathbf{F}_S$ can be decomposed into gravity and the normal force:

$$\mathbf{F}_S = \mathbf{F}_G + \mathbf{F}_N. \quad (18)$$

The *downhill force* acting parallel to the current trajectory $\mathbf{F}_P$ can be expressed as

$$\mathbf{F}_P = mg\,(\sin\gamma)\,\mathbf{e}_{\dot{\mathbf{r}}} = mg\,(\sin\alpha)\,(\sin\beta)\,\mathbf{e}_{\dot{\mathbf{r}}}, \quad (19)$$

where γ is the inclination angle of $\mathbf{e}_{\dot{\mathbf{r}}}$.

In the following, we investigate forces such as the *lateral force*, whose definition differs depending on whether the skier descends on a straight line or performs a turn. In the case of a straight line, we index these forces with lowercase letters (e.g., $\mathbf{F}_{\text{lat}}$). In the case of a turn, the index is uppercase (e.g., $\mathbf{F}_{\text{LAT}}$). Let us assume that the skier is descending on a straight line. Then the lateral force $\mathbf{F}_{\text{lat}}$ acting perpendicularly to the direction of travel is given as

$$\mathbf{F}_{\text{lat}} = \mathbf{F}_S - \mathbf{F}_P, \quad (20)$$

which is shown in Fig. 5. Should the skier perform a carved turn, the lateral force also includes a centripetal component $\mathbf{F}_C$, which yields

$$\mathbf{F}_{\text{LAT}} = \mathbf{F}_{\text{lat}} - \mathbf{F}_C. \quad (21)$$

The *centripetal force* $\mathbf{F}_C$ a skier is exposed to during turns can be expressed in terms of the lateral force as

$$\mathbf{F}_C = \frac{m}{R_{\text{sc}}}\|\dot{\mathbf{r}}\|^2 \frac{\mathbf{F}_{\text{lat}}}{\|\mathbf{F}_{\text{lat}}\|} \times \begin{cases} (+1) & \text{before crossing the fall line,} \\ (-1) & \text{after crossing the fall line,} \end{cases} \quad (22)$$

where m is the mass of the skier and R_{sc} is the sidecut radius of the skis, as introduced in Sec. II B. $\mathbf{F}_C$ is parallel to $\mathbf{F}_{\text{lat}}$ in the first half of the turn (before the skier crosses the fall line) and antiparallel to $\mathbf{F}_{\text{lat}}$ in the second half of the turn (after the skier has crossed the fall line). We refer to the force that has to be compensated for by the snow as the *effective force* $\mathbf{F}_{\text{eff}}$ of the skier. As shown in Fig. 6(a), the effective force is given as

$$\mathbf{F}_{\text{eff}} = \mathbf{F}_{\text{lat}} - \mathbf{F}_N \quad (23)$$

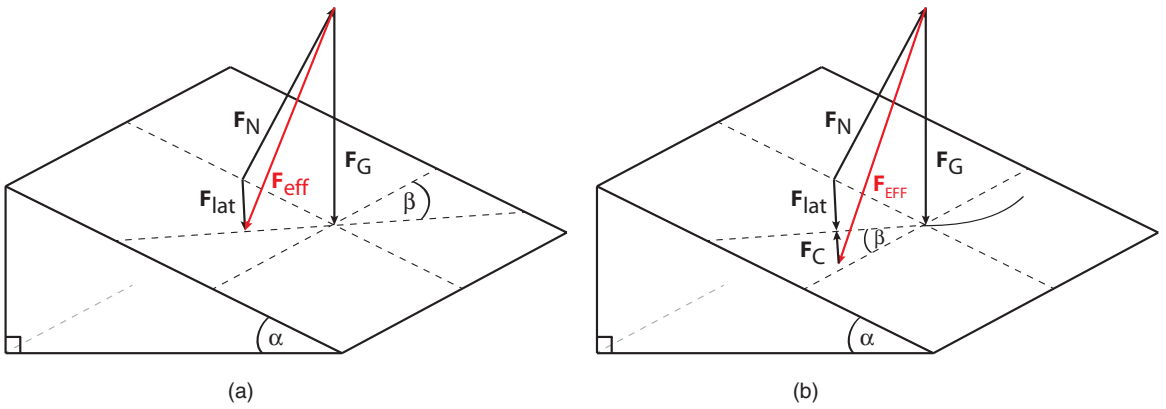

FIG. 6. (Color online) Effective force during the descent on a straight line (a) and a carved turn (b). (a) Skier descending in a straight line. The effective force can be determined as $\mathbf{F}_{\text{eff}} = \mathbf{F}_{\text{lat}} - \mathbf{F}_N$. (b) Skier performing the second half of a turn. The effective force can be determined as $\mathbf{F}_{\text{EFF}} = \mathbf{F}_{\text{lat}} - \mathbf{F}_N - \mathbf{F}_C$.

when the skier rides downhill on a straight line. In the case of carved turns, we obtain

$$\mathbf{F}_{\text{EFF}} = \mathbf{F}_{\text{LAT}} - \mathbf{F}_N = \mathbf{F}_{\text{lat}} - \mathbf{F}_N - \mathbf{F}_C \tag{24}$$

for the effective force $\mathbf{F}_{\text{EFF}}$ analogously [see Fig. 6(b)]. The *air drag* $\mathbf{F}_{\text{air}}$ a skier is exposed to is antiparallel to the current direction of motion $\mathbf{e}_{\dot{\mathbf{r}}}$ and can be expressed as

$$\mathbf{F}_{\text{air}} = -\tfrac{1}{2}\, C_d\, A\, \rho\, \|\dot{\mathbf{r}}\|^2\, \mathbf{e}_{\dot{\mathbf{r}}}, \tag{25}$$

where C_d is the dimensionless drag coefficient (which we assume to be independent of speed), ρ the air density, and A the projected frontal area of the skier perpendicular to $\mathbf{e}_{\dot{\mathbf{r}}}$ [39]. The *kinetic friction* $\mathbf{F}_{\text{ground}}$ decelerating the skier can be expressed in terms of the skier's effective force as

$$\mathbf{F}_{\text{ground}} = -\mu\, \|\mathbf{F}_{\text{eff}}\|\, \mathbf{e}_{\dot{\mathbf{r}}} \tag{26}$$

when descending on a straight line. Here, μ denotes the *kinetic friction coefficient* of skis on snow. In the case of a carved turn, we obtain

$$\mathbf{F}_{\text{GROUND}} = -\mu\, \|\mathbf{F}_{\text{EFF}}\|\, \mathbf{e}_{\dot{\mathbf{r}}} \tag{27}$$

analogously. Finally, the *net force* $\mathbf{F}_{\text{net}}$ accelerating the skier can be derived. Again, we have to distinguish between descents on straight lines and carved turns. In the case of no directional change, the net force is composed of the accelerating downhill force, as well as the decelerating air drag and kinetic friction:

$$\mathbf{F}_{\text{net}} = \mathbf{F}_P + \mathbf{F}_{\text{air}} + \mathbf{F}_{\text{ground}}. \tag{28}$$

During carved turns, the centripetal force $\mathbf{F}_C$ has to be taken into account as well, which yields

$$\mathbf{F}_{\text{NET}} = \mathbf{F}_P + \mathbf{F}_{\text{air}} + \mathbf{F}_{\text{GROUND}} + \mathbf{F}_C \tag{29}$$

for the net force $\mathbf{F}_{\text{NET}}$.

III. EXPERIMENT

High speed and density of skiers are two major factors increasing the risk and the severity of skiing accidents [30,31,40]. Knowing the regions on ski slopes that are prone to high speed and density is thus an important step toward accident prevention. We are therefore interested in how accurately our particle-based model can predict speed zones and densities occurring on real ski slopes. This section presents the results of an outdoor experiment we performed with 21 skiers with which the simulation output of our model can be compared. Section III A describes the experiment setup, and Sec. III B summarizes the results of the measurements. With the skier density being difficult to estimate with as few as 21 experiment participants, we focus on speed zones in the following.

A. Experimental setup

There are two major previous studies investigating the riding behavior of recreational skiers and snowboarders on ski slopes. Shealy *et al.* [41] measured the speed of some 650 individuals at three ski resorts in the United States with the help of radar speed guns. However, requiring the skiers traveling directly toward or away from them, which is hardly the case for skiers performing turns, the accuracy of the measurement results is limited. Thus, Schmitt *et al.* [42] determined the speed of around 6800 snow-sport athletes on one Swiss ski slope with the help of video-based tracking software. This approach, however, requires additional image processing such as sun-shade interface tracking and artifact suppression.

For our experiments, we selected the two slopes Graustock and Jochstock in the Swiss ski resort Engelberg, which can be considered as typical ski slopes and feature specialties such as narrowing and flattening parts, counter slopes, and steep sections. Corresponding pictures of the slopes are shown in Fig. 7. The lifts serving the two selected slopes have a maximum capacity of 2400 persons/h (Graustock) and 2800 persons/h (Jochstock) [43]. Table I summarizes more details on the two slopes. We conducted a 3-day experiment on these two slopes with seven skiers we chose randomly each day. All participants were experienced adult skiers with an average mass of about 85 kg including equipment. The visibility during these 3 days was unlimited (i.e., $d = \infty$), with an outside temperature of $\theta = -5\,^{\circ}\text{C}$. Finally, the slopes were free of obstacles.

To track their positions and speeds, the participants of our experiment carried an HTC Google Nexus One cell phone (Android version 2.2) with a built-in GPS receiver during the entire skiing day. The participants did not receive any further

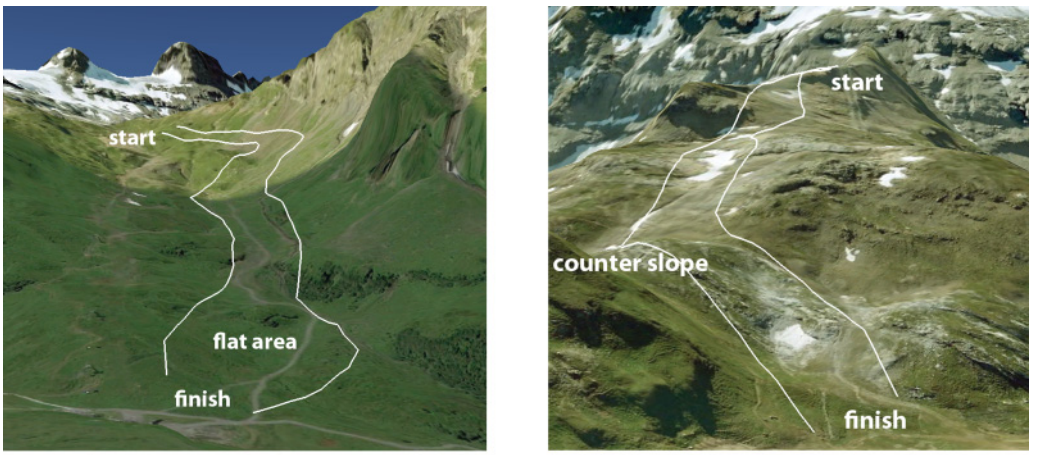

FIG. 7. (Color) Summer pictures of the two ski slopes at the ski resort Engelberg. (a) The slope Graustock is narrow at the beginning and gets wider. It flattens toward the end. (b) The slope Jochstock starts narrow and widens later on. Skiers also have to pass a counter slope.

instructions to avoid biased results. We lowered the sample rate of the internal GPS receiver from its maximum of 1.0 down to 0.33 Hz to reduce its energy consumption and make the batteries survive an entire skiing day. Blunck *et al.* [44] studied the GPS positioning accuracy of the HTC Nexus One. The 90 percentile p_{90} of the error distance ranges from 10 to 20 m, depending on the body placement of the cell phone. Position and speed data on the skiers participating in our experiment were recorded and stored with the help of the CoenoSense platform developed in-house [45]. CoenoSense can be used for distributed data recordings on mobile devices and consists of the two main components CoenoLogger and CoenoServer. CoenoLogger is an application running on all involved mobile devices, which records sensor values such as GPS data locally. All CoenoLoggers periodically transmit their recorded values through a cellular network to CoenoServer, a central repository, which collects and stores incoming data in a database [46].

B. Speed zones

Overall, we recorded 4100 s of location and speed data on the slope Graustock, which corresponds to 35 descents, and 3400 s on the slope Jochstock, which corresponds to 50 descents. Being interested in how fast skiers travel in various zones on a ski slope on average, we smoothed the speed data with a circular averaging linear filter with a radius of $r = 10$ m. That is, the average speed of the 21 skiers at each point of a slope was determined as the mean of all measured speed values within a distance of r. The resulting speed maps of the two slopes are presented in Fig. 8. A closer look at these two diagrams reveals that the skiers require some time to accelerate at the beginning of slopes, until they reach their average traveling speed. As expected, flattening slopes and counter slopes enforce a remarkable speed loss [see Fig. 8(b)]. Figure 9 shows the distribution of the measured speed for the two slopes. Apparently, skiers descend more slowly and sometimes even stop on the slope Graustock. This might be due to the fact that this slope is classified as being more difficult than Jochstock (see Table I).

TABLE I. Characterization of the two ski slopes at Engelberg.

	Graustock	Jochstock
Difficulty rating	Expert	Intermediate
Length (m)	1250	889
Average width (m)	81	62
Altitude at start (m)	2178	2504
Altitude difference (m)	413	288
Average inclination (%)	33	32
Maximum lift capacity (persons/h)	2400	2800

IV. SIMULATIONS

This section summarizes the major results obtained by computer simulations of the traffic model presented in Sec. II. Section IV A describes our simulation framework. Section IV B summarizes the choices we made for the values of the simulation input parameters. Section IV C compares the simulation output with the measurements of the on-slope experiment. A factor especially increasing the risk of collisions is a high density of skiers on a slope [31]. We therefore demonstrate how our simulation tool can be used to predict skier densities in Sec. IV D. Section IV E compares recorded and simulated trajectories of several skiers. Finally, Sec. IV F studies the relationship among the density, speed, and flow of skiers in three typical scenarios.

A. Simulation framework

We implemented the traffic model as a simulation framework for Matlab as introduced in Sec. II. The simulations were run on a Sun Fire X2200M2 Quad Core server. During the descent on a slope, each skier is accelerated by the physical force $\mathbf{F}_{\text{net}}(t)$. To evolve their corresponding motions over time, we apply Gear's predictor-corrector algorithm, which is routinely used in molecular dynamics [47,48]. As a compromise between accuracy and computational efficiency, we choose an integration step size of 10 ms. Each run simulates 1 h of skiing traffic on the specified slope.

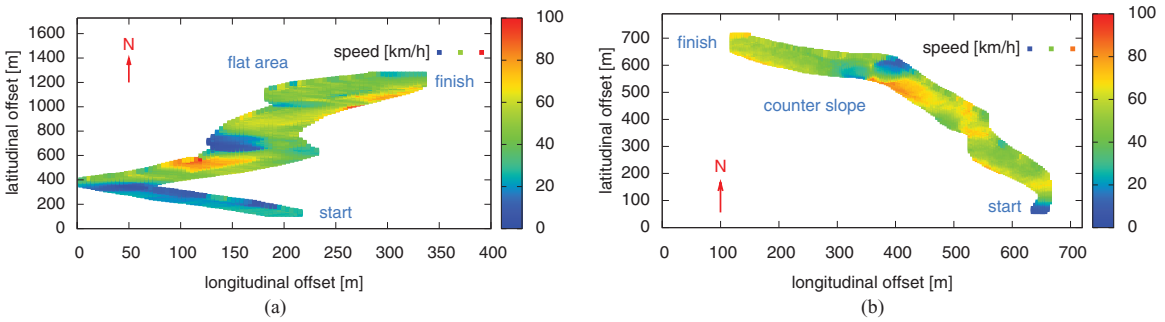

FIG. 8. (Color) Average speed measured during the experiment. The speed at each point of a slope was determined as the mean of all measured values observed within a distance of 10 m. The slopes are visualized in top view. As we might expect, skiers need some time to reach their traveling speed. Moreover, flattening (a) and counter slopes (b) slow them down. (a) Average speed of 35 descents on Graustock. (b) Average speed of 50 descents on Jochstock.

B. Parameter selection

There are four types of parameters the simulation framework takes as input: parameters describing the ski slope (such as its elevation model), parameters for the social forces, fixed parameters for the physical forces given by the experiment conditions (such as the outside temperature), and free parameters for the physical forces that have to be estimated from the recordings (such as the kinetic friction coefficient).

Altitude data for the two ski slopes were obtained from the Swiss Federal Office of Topography, which maintains a digital elevation model of Switzerland with a resolution of 2×2 m and an altitude precision of 0.5 m [49]. We assume that skiers arrive at the beginning of the slopes at a constant rate λ and start their descents at a typical walking speed of $v_{\min} = 5$ km/h. The lifts serving the two selected slopes have a maximum capacity of 2400 persons/h (Graustock) and 2800 persons/h (Jochstock) [43]. Considering the fact that the lifts do not normally operate at full capacity and that skiers spread across several available trails upon arrival, we choose an arrival rate of $\lambda = 600$ persons/h for both slopes. With the simulated time being 1 h, each simulation run covers the descents of 600 skiers.

As presented by Helbing [14], we assume that the repulsive potentials defining the social forces from Sec. II C decrease exponentially as

$$U(\|\mathbf{r}_{aL}\|) = U_0 \exp(-\|\mathbf{r}_{aL}\|/R_L), \tag{30}$$

$$U(\|\mathbf{r}_{aR}\|) = U_0 \exp(-\|\mathbf{r}_{aR}\|/R_R), \tag{31}$$

$$V(s) = V_0 \exp(-s/R_A), \tag{32}$$

where R_L, R_R, and R_A denote the ranges of the social repulsions, and U_0 and V_0 the interaction strengths between skier a and the respective object. With the ski slopes having been free of obstacles during the experiments, we ignore the obstacle repulsion. As mentioned in Sec. II, the social forces of our model only determine the desired direction $\mathbf{e}_{\text{social}}$ of skiers and do not accelerate them. The social forces are thus dimensionless, and only their relative strengths count. To obtain interactional forces with a realistic range and equivalent strengths, we choose $A_0 = 1$ for the destination force, $U_0 = 1$, $V_0 = 100$, $R_L = R_R = 50$, and $R_A = 2$. This selection of values has the following practical implications: the magnitude of the destination force is always 1, or $\|\mathbf{F}_D\| = 1$. The magnitude of the edge repelling force converges to 1 when a skier approaches an edge. It drops down to $\|\mathbf{F}_L\| = 0.6$ when the skier is 50 m away from an edge. The magnitude of the repulsion of skier a from skier b is 1 if b is 9 m away from a and b approaches a at a speed of 20 km/h. It drops down to $\|\mathbf{F}_A\| = 0.005$ when skier b is 20 m away from skier a. We set the angle of view to $2\varphi = 180^\circ$, which roughly corresponds to that of the human eye [50]. According to Fig. 3, simulated skiers only perform a turn when the angle between the current direction of motion and the desired direction exceeds the threshold angle δ. We set $\delta = 10^\circ$. Table II

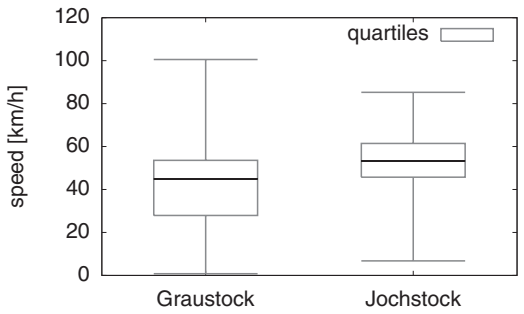

FIG. 9. Speed distribution measured during the experiment (min, p_{25}, p_{50}, p_{75}, max). Apparently, skiers descend more slowly and sometimes even stop on Graustock. This might be due to the fact that this slope is classified as being more difficult than Jochstock (see Table I).

TABLE II. Values selected for the parameters of the social forces.

Parameter	Symbol	Our choice
Strength of destination force	A_0	1
Strength of edge repulsion	U_0	1
Strength of athlete repulsion	V_0	100
Range of edge repulsion	$R_L = R_R$	50
Range of athlete repulsion	R_A	2
Angle of view	2φ	180°
Directional deviation	δ	10°

TABLE III. Fixed simulation parameters adjusted to the experimental conditions.

Parameter	Symbol	Value
Visibility	d	∞
Temperature	θ	-5 °C
Air density	ρ_{air}	1.3163 kg/m^3
Skier mass	m	85 kg
Gravitational acceleration	g	9.81 m/s^2

summarizes the choices we made for the parameters of the social forces. As presented in Sec. II, downhill routes of skiers can be parametrized by waypoints skiers want to reach during their descent. For our simulations, we assume that skiers choose these waypoints randomly every 50 m, using a uniform distribution on the corresponding line from the left to the right edge of the slope.

We adjust the fixed simulation parameters to the experimental conditions at Engelberg. In correspondence with the experiment, we assume a clear sky with an unlimited visibility $d = \infty$ and an outside temperature of $\theta = -5$ °C. The density of air is $\rho_{\text{air}} = 1.3163$ kg/m^{-3} at -5 °C. We set the mass of the skiers to $m = 85$ kg, which includes clothes and equipment. The gravitational acceleration of the Earth is $g = 9.81$ m/s in Switzerland. Table III summarizes the fixed parameters.

For a first simulation run, we initialize the free simulation parameters with values commonly known from the literature [35,51–54]. The sidecut radius of modern carving skis, introduced in Sec. II A, is designed for a turn radius ranging from 7 to 15 m [35]. Studies on ski slopes confirm that skiers perform turns with an equivalent radius [42]. We choose a sporty sidecut radius of $R_{\text{sc}} = 10$ m. Studies have revealed that skiers skiing the fall line are subject to a kinetic friction coefficient of $\mu = 0.02$ [51]. Descending in turns increases this coefficient to values between 0.05 and 0.15 [53]. As the skiers in our simulation perform turns regularly, we choose $\mu = 0.1$ for the simulations. For simplicity, we assume that this value does not depend on the difficulty of the terrain or the skills of the skiers. Values ranging from 0.5 to 1.4 are reported for the air drag coefficient C_d of skiers by various research groups [52,54]. We choose a typical value of $C_d = 1.0$ and assume that it is independent of the speed of the skier. The

TABLE IV. Free simulation parameters initialized with values from the literature [35,51–54].

Parameter	Symbol	Range	Our choice
Sidecut radius	R_{sc}	[7 m, 15 m]	10 m
Kinetic friction coefficient	μ	[0.05,0.15]	0.1
Drag coefficient	C_d	[0.5,1.4]	1.0
Frontal area	A	[0.3 m^2,0.9 m^2]	0.6 m^2

frontal area A of skiers has been studied widely. Determined values range from 0.3 m^2 in a tuck position up to 0.9 m^2 in a fully upright position [52,54]. We select $A = 0.6$ m^2 for our simulations. Table IV summarizes the value ranges of the free simulation parameter as well as our initial choices.

C. Speed zones

One important factor for accidents is the high speed of snow-sport athletes. It can lead to a loss of control of skiers and thus increases the risk of accidents [30,40]. Knowing how fast skiers travel in various areas on ski slopes is therefore an important step toward accident prevention. In the following, we investigate how accurately our simulation predicts speed zones at the example of the two ski slopes Graustock and Jochstock.

In accordance with the processing of the measurement data, we determined the speed at each point of the slopes as the average speed of all 600 simulated skiers observed within a distance of $r = 10$ m. The corresponding speed maps are presented in Fig. 10 and reveal the following: as measured during the experiments, the skiers need some time to reach their traveling speed. Moreover, flattening slopes [see Fig. 10(a)] and counter slopes [see Fig. 10(b)] slow the skiers down.

The signed relative error of the simulated with respect to the measured speed is shown in Fig. 11. While there is a good overall correspondence for Jochstock [see Fig. 11(b)], some regions on Graustock show significant differences [see Fig. 11(a)]. One reason for this discrepancy is skiers slowing down deliberately due to the more difficult terrain of the expert slope Graustock. Overall, the median of the signed relative speed error is $p_{50} = 16.9\%$ for Graustock and $p_{50} = -0.15\%$ for Jochstock. The median of the unsigned relative speed error is $p_{50} = 26.8\%$ for Graustock and $p_{50} = 14.9\%$ for Jochstock.

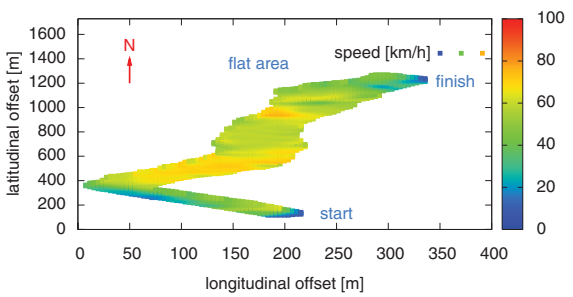

(a) Average speed of 600 skiers on *Graustock*.

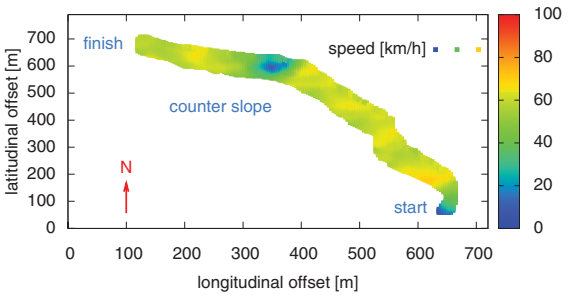

(b) Average speed of 600 skiers on *Jochstock*.

FIG. 10. (Color) The speed for each point on the two slopes was determined as the average speed of all 600 simulated skiers observed within a distance of 10 m. The simulations confirm the observations in the experiment: skiers need some time to accelerate and are slowed down by flat areas (a) and counter slopes (b). Average speed of 600 skiers on (a) Graustock and (b) Jochstock.

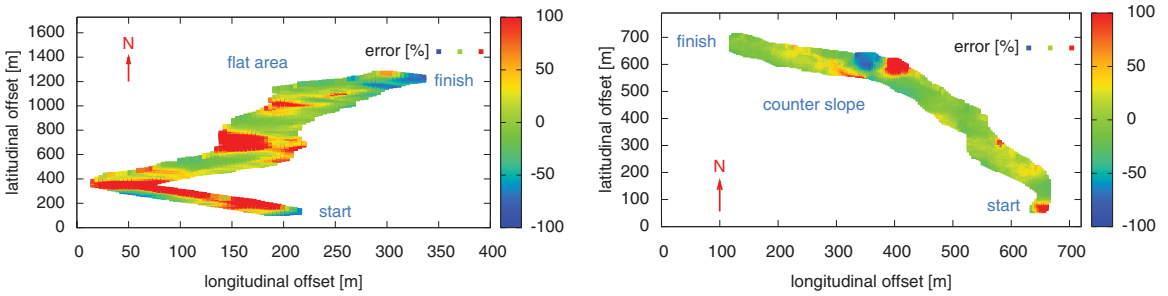

(a) Relative speed error for *Graustock*.

(b) Relative speed error for *Jochstock*.

FIG. 11. (Color) Signed relative error of the simulated with respect to the measured average speed. There are some regions on Graustock with significant speed differences (a), whereas there is a good overall correspondence for the slope Jochstock (b). Relative speed error for (a) Graustock and (b) Jochstock.

Figure 12 compares the measured and simulated speed distributions. As for Graustock, we measured an average speed of 42.1 km/h (standard deviation $\sigma = 17.5$ km/h) and obtained 54.1 km/h ($\sigma = 13.4$ km/h) in the simulation. As for Jochstock, we measured an average speed of 51.8 km/h ($\sigma = 14.3$ km/h) and obtained 55.2 km/h ($\sigma = 11.4$ km/h) in the simulation. Apparently, the simulated speed is higher and less dispersed than the measured one on both slopes.

D. Skier density

As mentioned earlier, a factor especially increasing the risk of collisions is a high density of skiers on ski slopes [31]. We are therefore interested in predicting zones with an increased number of skiers with our simulation tool. To do so, we determined the skier density for each position on the two slopes as the average number of skiers within a distance of $r = 10$ m.

Figure 13 shows the resulting density maps of the slopes. Apparently, skiers prefer the center of the slopes and try to keep away from the edges. Moreover, the skier density increases with decreasing width of the slopes. It also increases when skiers start slowing down due to the terrain. This behavior can, for example, be observed in flat areas [see Fig. 13(a)] or before counter slopes [see Fig. 13(b)]. To reduce the amount of skiing traffic and thus the risk of accidents, slope operators could, for example, widen the slope in zones for which our simulation tool predicts a high density.

E. Trajectory analysis

A comparison of recorded and simulated trajectories of skiers on the two slopes is shown in Fig. 14. Apparently, the participants of the experiment pass the edges of the slopes from time to time [see Fig. 14(a)]. Moreover, they perform fewer turns than the skiers in the simulations. On average, the skiers perform 2.7 turns every 100 m in the experiment and 3.4 turns in the simulation on Graustock. As for Jochstock, the skiers perform 2.0 turns every 100 m in the experiment and 3.6 turns in the simulation. Figure 15 shows a spatial distribution of the average number of turns per skier during the experiment and the simulations. Apparently, the skiers perform more turns when the density increases due to speed loss in flat areas and narrow sections. In the experiment, the skiers turn more frequently on Graustock than on Jochstock, most likely to better control their speed on the expert slope. On the contrary, the average number of turns per skier is more or less the same for both slopes in the simulations, as the dominating factor for turns is the selection of waypoints, which is independent of the slope terrain.

Another parameter describing the trajectories is the distribution of the angle κ between the trajectory and the fall line. The smaller the mean of κ, the more directly skiers descend the slope. As for Graustock, the mean of κ is 21.5° in the experiment and 19.9° in the simulation. As for Jochstock, the mean of κ is 16.8° in the experiment and 15.9° in the

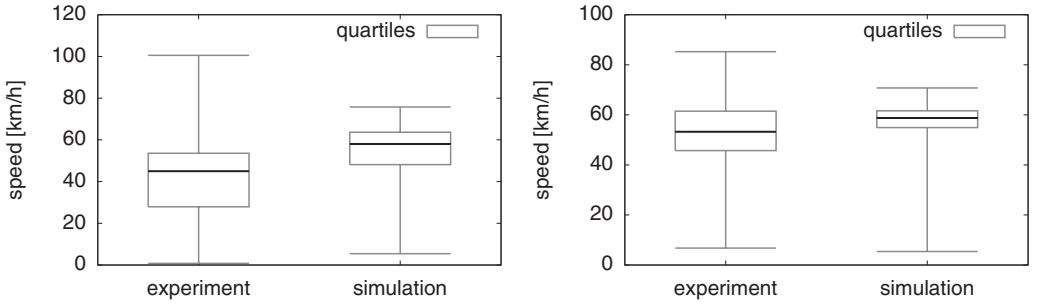

(a) Speed distribution on *Graustock*.

(b) Speed distribution on *Jochstock*.

FIG. 12. Speed distribution in experiment and simulation (min, p_{25}, p_{50}, p_{75}, max). Apparently, the simulated speed is higher and less dispersed than the measured one on both slopes. The skiers in the simulation have a minimal initial speed of 5 km/h. Speed distribution on (a) Graustock and (b) Jochstock.

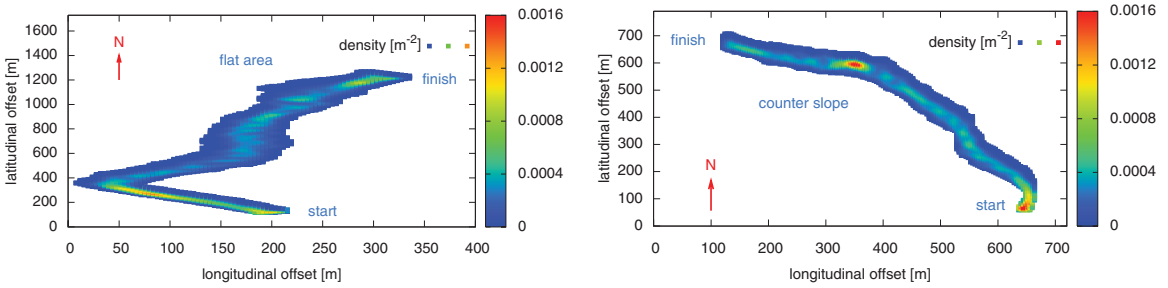

(a) Skier density on *Graustock*.

(b) Skier density on *Jochstock*.

FIG. 13. (Color) Maps of skier densities occurring on the two slopes. Skiers prefer riding in the center of the slopes. The density increases when the slope narrows and when skiers slow down due to flat areas (a) or counter slopes (b). Skier density on (a) Graustock and (b) Jochstock.

simulation. Figure 16 shows a spatial distribution of κ. In the experiment, the skiers deviate more from the fall line on Graustock than on Jochstock, most likely to decrease the acceleration on the expert slope.

F. Fundamental diagrams of traffic flow

To understand the emergence of congestion on ski slopes, we determined the relation among the density ρ, the average speed v, and the flow J of skiers in different scenarios on the slope Jochstock. The start of the slope, a typical downhill section, and a section containing a counter slope were selected as areas of interest. As in Sec. IV E, these areas on the slope have a length of 100 m. We varied the arrival rates of skiers from 300 up to 3600 persons/h, which is greater than the maximum capacity of 2800 persons/h of the corresponding ski lift. The resulting fundamental diagrams of traffic flow are shown in Fig. 17. Apparently, an increase in the skier density forces skiers to slow down [see Fig. 17(a)]. However, the skiers do not stop and congestion does not even occur at an arrival rate exceeding the capacity of the ski lift. This observation is also confirmed by a density-flow diagram [see Fig. 17(a)].

V. PARAMETER SENSITIVITY ANALYSIS

We were able to show a good correspondence of the simulation with measurements by initializing the simulation input parameters with values from the literature. Intuitively, the question arises as to how robust our traffic model is against the variation of these parameters. In a sensitivity analysis, we therefore assessed the influence of all input parameters on the predicted speed and density by exploring reasonable parameter spaces with a linear parameter sweep. The analysis reveals that the model responds to the variation of the parameters as follows.

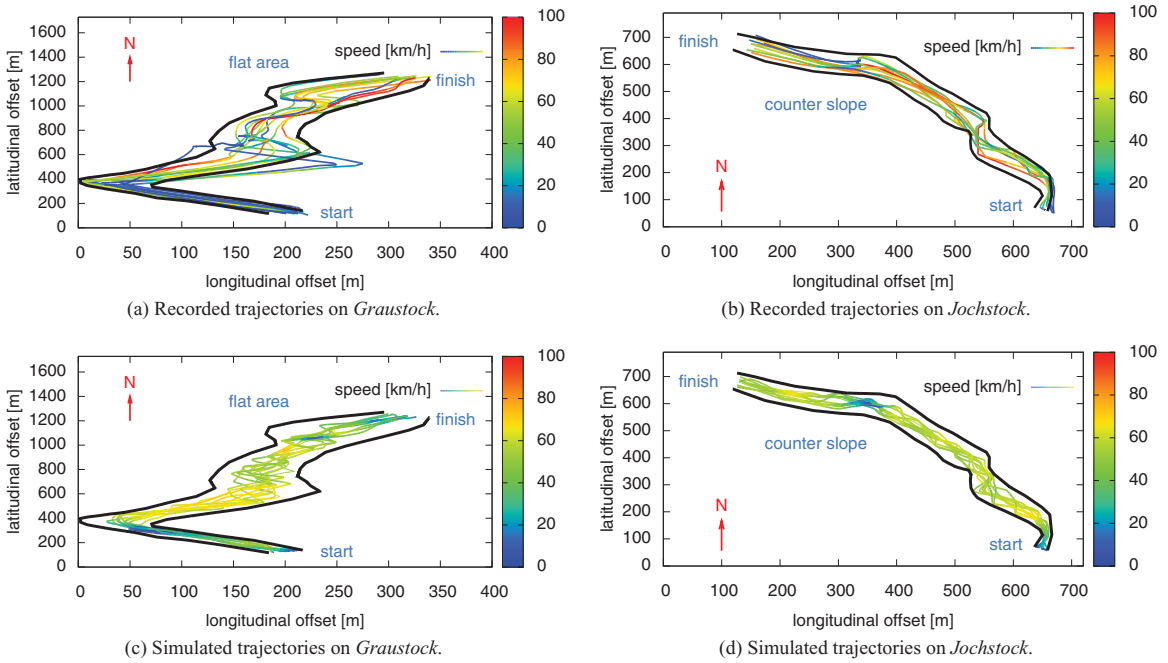

(a) Recorded trajectories on *Graustock*.

(b) Recorded trajectories on *Jochstock*.

(c) Simulated trajectories on *Graustock*.

(d) Simulated trajectories on *Jochstock*.

FIG. 14. (Color) Recorded (a, b) and simulated (c, d) trajectories of 10 skiers on the two slopes. Apparently, the skiers pass the edges of the slopes from time to time during the experiment (a). Moreover, they perform fewer turns and prefer more direct descents in reality. Recorded trajectories on (a) Graustock and (b) Jochstock. Simulated trajectories on (c) Graustock and (d) Jochstock.

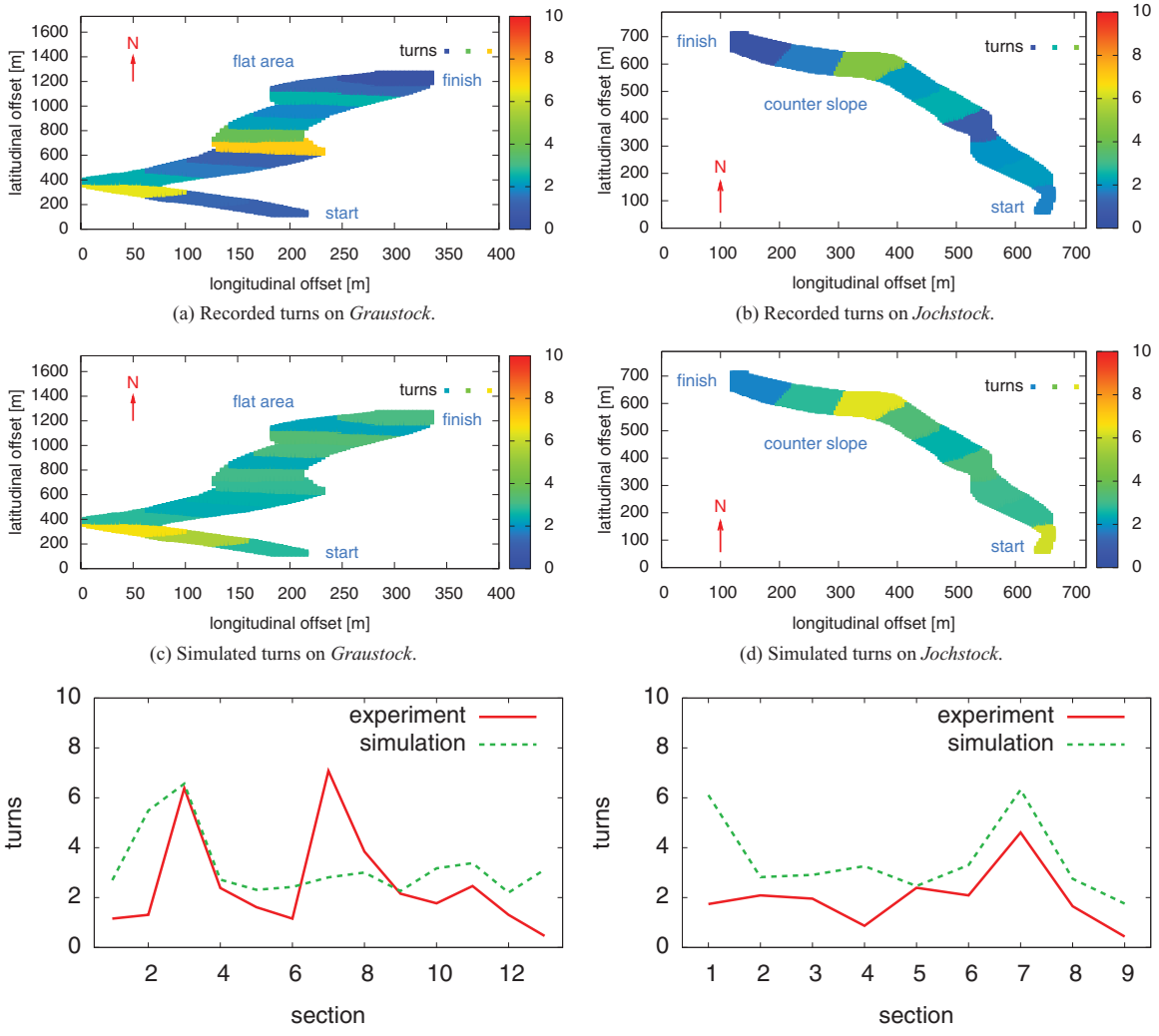

(a) Recorded turns on *Graustock*.

(b) Recorded turns on *Jochstock*.

(c) Simulated turns on *Graustock*.

(d) Simulated turns on *Jochstock*.

(e) Recorded and simulated turns on *Graustock*.

(f) Recorded and simulated turns on *Jochstock*.

FIG. 15. (Color) To obtain a spatial distribution of the average number of turns per skier, we split the slopes into sections 100 m in length. Apparently, the skiers perform more turns when the density increases due to speed loss in flat areas and narrow sections. In the experiment, the skiers perform more turns on Graustock than on Jochstock, most likely to better control their speed on the expert slope. Recorded turns on (a) Graustock and (b) Jochstock. Simulated turns on (c) Graustock and (d) Jochstock. Recorded and simulated turns on (e) Graustock and (f) Jochstock.

(1) The variation of the threshold angle δ, which determines when skiers perform turns, has just a marginal influence on the simulated speed and density. The relative speed error reaches a minimum at $\delta = 10^{\circ}$.

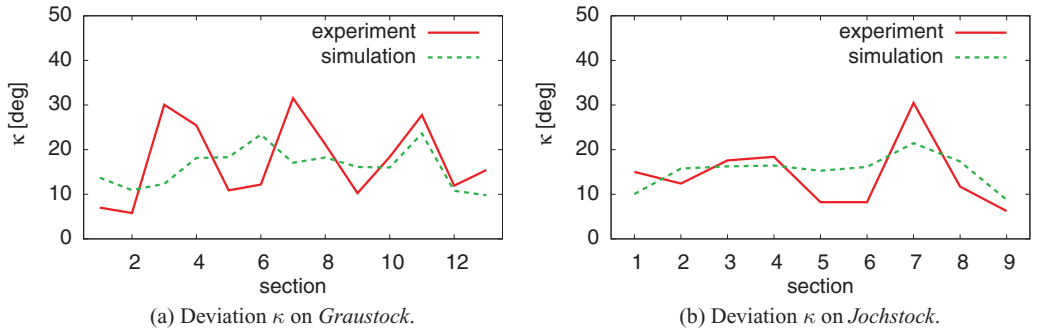

(a) Deviation κ on *Graustock*.

(b) Deviation κ on *Jochstock*.

FIG. 16. (Color online) To obtain a spatial distribution of the mean of κ, we split the slopes into sections 100 m in length. In the experiment, the skiers deviate more from the fall line on Graustock than on Jochstock, most likely to decrease the acceleration on the expert slope. (a) Deviation κ on (a) Graustock and (b) Jochstock.

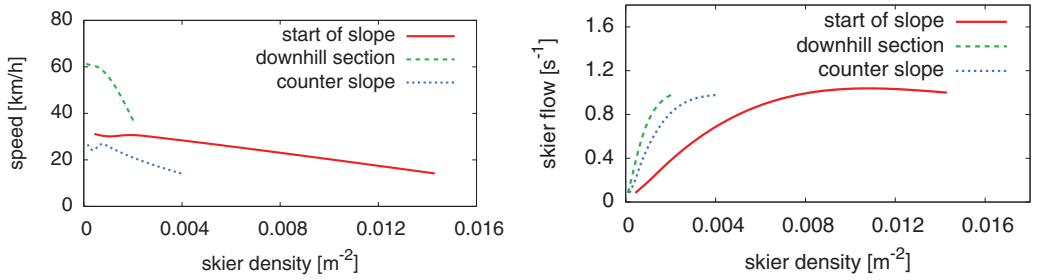

FIG. 17. (Color online) Fundamental diagrams of traffic for three sections on Jochstock. Apparently, an increase in the skier density forces skiers to slow down. However, skiers do not stop and congestion does not even occur at an arrival rate exceeding the capacity of the corresponding ski lift. (a) Speed depending on the skier density. (b) Skier flow depending on the skier density.

(2) Only the arrival rate λ of skiers and the ranges R_L, R_R, and R_A of the edge and athlete repulsion influence the simulated skier density. The more skiers arrive at the start of the slope, the higher the densities will be. However, the spots with an increased density, such as areas before counter slopes, are independent of λ.

Increasing the ranges R_L and R_R of the edge repulsion forces skiers to keep farther away from the edges. Figure 18 shows the effect of increasing the range R_A of the athlete repulsion on the riding behavior of skiers. When skiers start slowing down at the counter slope, skiers approaching from behind are repelled earlier and try to keep away by riding toward the edges. This becomes obvious when looking at the trajectories of several consecutive skiers [see Figs. 18(c) and 18(d)].

(3) The simulated speed is influenced by the skier mass m, the kinetic friction coefficient μ, and the arrival rate λ. Figure 19(a) shows that the simulated speed increases with increasing mass. Moreover, Fig. 19(b) illustrates that the simulated speed decreases with increasing μ. As shown in Sec. IV F, the speed also decreases with an increasing number of skiers on the slope.

The mass m of the skiers is not a free simulation parameter, but given by the experiment. We therefore restrict ourselves to study of the effect of varying μ on the simulated relative speed error, which is shown in Fig. 20. The median of the error reaches a minimum at $\mu = 0.125$ for Graustock and at $\mu = 0.1$ for Jochstock. Apparently, the participants in our experiment slow down more on Graustock. This might be due to the fact that the terrain of this slope is classified as more difficult than

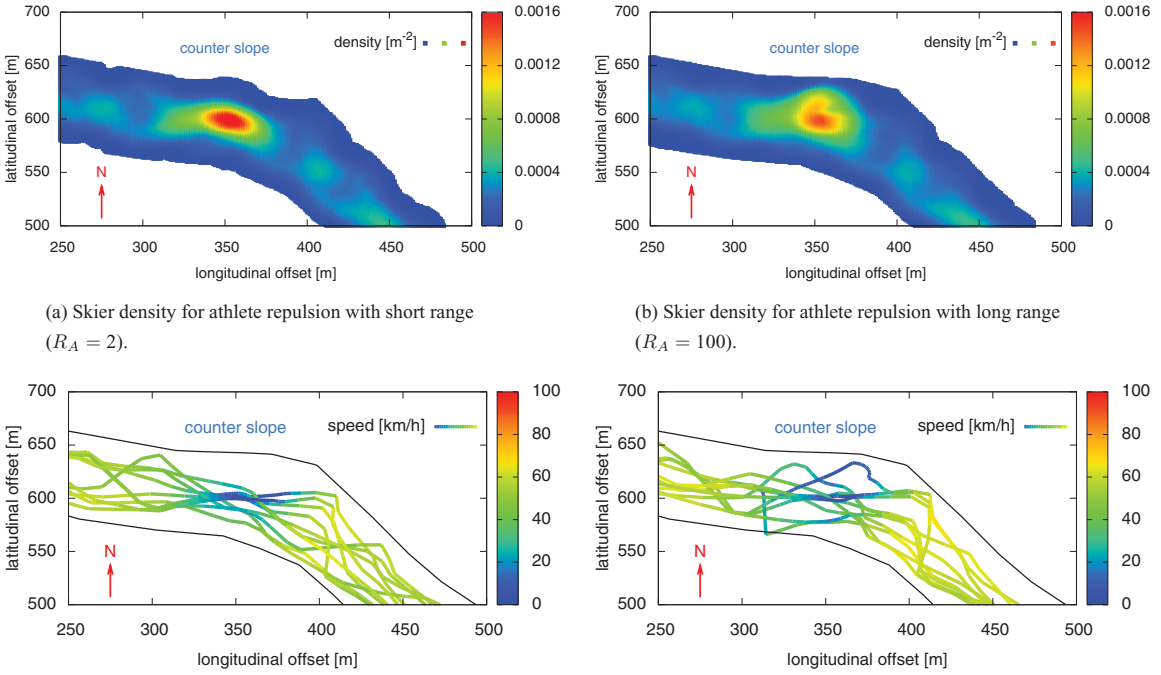

(a) Skier density for athlete repulsion with short range ($R_A = 2$).

(b) Skier density for athlete repulsion with long range ($R_A = 100$).

(c) Trajectories of 10 consecutive skiers for athlete repulsion with short range ($R_A = 2$).

(d) Trajectories of 10 consecutive skiers for athlete repulsion with long range ($R_A = 100$).

FIG. 18. (Color) Effect of increasing the range R_A of the athlete repulsion on Jochstock. When skiers start slowing down at the counter slope, other snow-sport athletes approaching from behind are repelled earlier and try to keep away by riding toward the edges (b, d). Skier density for (a) athlete repulsion with a short range ($R_A = 2$) and (b) athlete repulsion with a long range ($R_A = 100$). Trajectories of 10 consecutive skiers for (c) athlete repulsion with a short range ($R_A = 2$) and (d) athlete repulsion with a long range ($R_A = 100$).

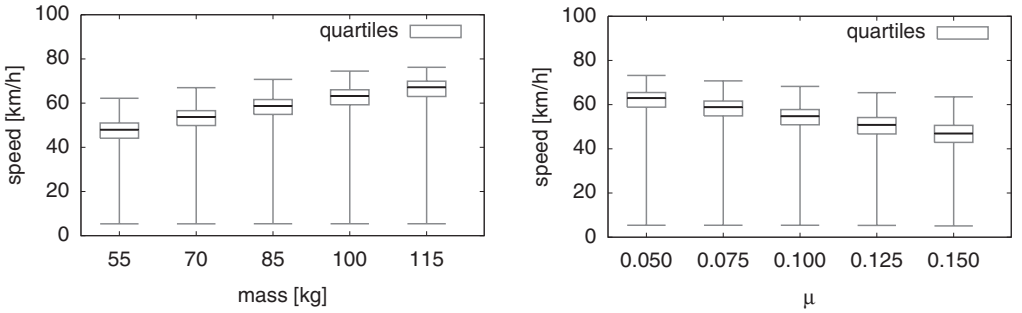

(a) The simulated speed increases with increasing m.

(b) The simulated speed decreases with increasing μ.

FIG. 19. Influence of (a) m and (b) μ on the speed distribution (min, p_{25}, p_{50}, p_{75}, max) on Jochstock. Skiers have a minimal initial speed of 5 km/h. The simulated speed (a) increases with increasing m and (b) decreases with increasing μ.

Jochstock. Another reason could be different snow conditions on the two slopes.

Apparently, we cannot achieve a perfect match between reality and simulation with the variation of μ. There are two interpretations of that observations. On the one hand, we have assumed that μ is constant in all situations. In reality, however, μ varies depending on the snow conditions and the skills of the skiers. On the other hand, there are other parameters having an effect on the simulated speed, which are not included in the sensitivity analysis, such as the selection of waypoints. For example, we suppose skiers choose waypoints randomly, which is an assumption that does not always hold in reality.

VI. CONCLUSION AND OUTLOOK

In recent decades, numerous models for the traffic of vehicles, pedestrians, and animal swarms have been developed with the goal of studying the emergence of congestion and panic situations. The methods to model these scenarios range from macroscopic to mesoscopic and microscopic (particle-based) approaches. Although everyday systems have already been investigated thoroughly, the field of traffic in sports, especially skiing, remains largely unexplored. We have therefore developed a particle-based traffic model, which

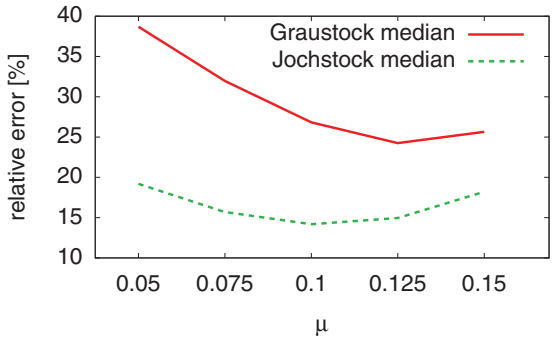

FIG. 20. (Color online) Median of the unsigned relative speed error depending on the kinetic friction coefficient μ. The median of the relative error reaches a minimum at $\mu = 0.125$ for Graustock and at $\mu = 0.1$ for Jochstock. Apparently, the participants in our experiment slow down more on Graustock. This might be due to the fact that the terrain of this slope is classified as more difficult than Jochstock. Another reason could be different snow conditions on the two slopes.

describes the individual riding behavior of skiers and the interaction between skiers on ski slopes on a given topography. We model skiers as particles with a mass that are exposed to so-called social forces attracting skiers to desired waypoints and repelling them from the edges of the slope, obstacles, and other skiers. These social forces can be considered as an internal motivation of skiers to perform certain movements. The superposition of all social forces that skiers are exposed to indicates their desired direction of motion. Physical forces such as gravitational and centripetal forces as well as the kinetic friction and the air drag accelerate and decelerate skiers toward their desired directions.

We recorded position and speed data of 21 skiers with GPS-equipped cell phones on two ski slopes and showed the validity of our model by comparing the measured speeds with the speeds resulting from computer simulations of our model, which yielded a good overall correspondence. Our experiment and simulations show that skiers slow down due to terrain, for example, in flat areas and on counter slopes. Moreover, high densities of skiers can be expected when skiers slow down and when slopes narrow. We determined the effect of varying the model input parameters on the simulation results in a sensitivity analysis. The ranges of the repelling social forces shape the density of skiers on the slope, whereas the speed is mainly influenced by the skier mass, the dynamic friction coefficient for skis on snow, and the arrival rate of skiers. All in all, our traffic model allows for the prediction of speed zones and skier densities occurring on ski slopes, which is important for the safe design of trails. For example, slope operators could widen slopes in regions with a predicted increased skier density. Our traffic model is thus likely to be advantageous in the prevention of accidents on ski slopes.

So far, our simulations have assumed the ski slopes are free of obstacles. Future simulations will investigate and evaluate the influence of obstacles on speed and density as well. We are currently extending our model by a new algorithm, which describes the waypoint selection of skiers more realistically. Occasionally, skiers tend to take into account their environment when choosing waypoints rather than selecting them randomly. For example, they avoid making any decelerating turns before counter slopes and in flat zones to gain a maximum of speed. Moreover, we introduce a maximum speed for skiers that they do not exceed during their descents. The maximum speed is an individual parameter for each skier and depends on the skier's personal skills and weather conditions. For

example, skiers will choose a lower traveling speed when the visibility is limited due to foggy weather. The comparison between experiment and simulation showed that the behavior of skiers is nonhomogeneous in reality: the speeds that real skiers choose are more dispersed than in our simulation. One way to model this observation more realistically is to make the only free parameter controlling the speed variable. Up to now, we have assumed that the kinetic friction coefficient μ is constant for all skiers and situations on ski slopes. Usually, however, μ is subject to snow conditions as well as the turning technique used and the underlying terrain. For example, skiers are much more likely to slow down in steep areas than on flat and easy trails. In the future, we will collect empirical data on skier densities on the two slopes to validate the accuracy of the density prediction as well.

ACKNOWLEDGMENTS

The authors would like to thank Annemarie Holleczek (University of Oxford) for many helpful discussions. Moreover, the authors thank Martin Wirz (ETH Zurich) for the organization of the data recording session on the ski slopes in Engelberg. Many thanks also go to Google for providing us with cell phones.

[1] T. Nagatani, Rep. Prog. Phys. **65**, 1331 (2002).
[2] A. Pipes, J. Appl. Phys. **24**, 274 (1953).
[3] M. Lighthill and G. Whitham, Proc. R. Soc. London A **229**, 317 (1955).
[4] K. Nagel and M. Schreckenberg, J. Phys. I (France) **2**, 2221 (1992).
[5] O. Biham, A. A. Middleton, and D. Levine, Phys. Rev. A **46**, 6124 (1992).
[6] B. S. Kerner and P. Konhäuser, Phys. Rev. E **48**, 2335 (1993).
[7] B. S. Kerner and P. Konhäuser, Phys. Rev. E **50**, 54 (1994).
[8] D. Helbing and B. Huberman, Nature **396**, 738 (1998).
[9] H. Y. Lee, H.-W. Lee, and D. Kim, Phys. Rev. Lett. **81**, 1130 (1998).
[10] M. R. Flynn, A. R. Kasimov, J.-C. Nave, R. R. Rosales, and B. Seibold, Phys. Rev. E **79**, 056113 (2009).
[11] M. Kanai, Phys. Rev. E **82**, 066107 (2010).
[12] L. Henderson, Nature **229**, 381 (1971).
[13] L. Henderson and D. Lyons, Nature **240**, 353 (1972).
[14] D. Helbing and P. Molnar, Phys. Rev. E **51**, 4282 (1995).
[15] D. Helbing and M. Treiber, Science **282**, 2001 (1998).
[16] M. Schreckenberg and S. Sharma, eds., *Pedestrian and Evacuation Dynamics* (Springer, Berlin, 2001).
[17] D. Yanagisawa, A. Kimura, A. Tomoeda, R. Nishi, Y. Suma, K. Ohtsuka, and K. Nishinari, Phys. Rev. E **80**, 036110 (2009).
[18] Q.-Y. Hao, M.-B. Hu, X.-Q. Cheng, W.-G. Song, R. Jiang, and Q.-S. Wu, Phys. Rev. E **82**, 057602 (2010).
[19] G. Baglietto and D. Parisi, Phys. Rev. E **83**, 056117 (2011).
[20] C. Reynolds, Comput. Graphics **21**, 25 (1987).
[21] T. Vicsek, A. Czirók, E. Ben-Jacob, I. Cohen, and O. Shochet, Phys. Rev. Lett. **75**, 1226 (1995).
[22] I. Prigogine and R. Herman, *Kinetic Theory of Vehicular Traffic* (Elsevier, New York, 1971).
[23] D. Helbing, Rev. Mod. Phys. **73**, 1067 (2001).
[24] A. Subic, P. Clifton, and J. Beneyeto-Ferre, in *The Engineering of Sport 7*, Vol. 1 (Springer, New York, 2008).
[25] E. Pino and M. Colville, Am. J. Sports Med. **17**, 778 (1989).
[26] R. B. Abu-Laban, Canadian. Med. Assoc. J. **145**, 1097 (1991).
[27] C. Bladin, P. Giddings, and M. Robinson, Am. J. Sports Med. **21**, 701 (1993).
[28] A. Sutherland and S. Myers, Injury **27**, 423 (1996).
[29] C. Made and L. Elmqvist, Scand. J. Med. Sci. Sports **14**, 128 (2004).
[30] National Ski Areas Association (NSAA), Facts about skiing/snowboarding safety; available at: [http://www.nsaa.org/nsaa/press/facts-ski-snbd-safety.asp]. Accessed February 15, 2010.
[31] L. Laskowski-Jones and L. Jones, Nursing2009 **39**, 24 (2009).
[32] D. Helbing and A. Johansson, in *Extreme Environmental Events*, edited by R. Meyers (Springer, New York, 2011), pp. 697–716.
[33] A. Renshaw and C. Mote Jr., Int. J. Mech. Sci. **31**, 721 (1989).
[34] U. Jentschura and F. Fahrbach, Can. J. Phys. **82**, 249 (2004).
[35] S. Masia, Skiing Heritage J. **17**, 33 (2005).
[36] K. Lewin, *Field Theory in Social Science* (Harper, New York, 1951).
[37] D. Helbing, J. Math. Sociol. **19**, 189 (1994).
[38] D. Lind and S. Sanders, *The Physics of Skiing*, 2nd ed. (Springer, New York, 2004).
[39] K. Watanabe and T. Ohtsuki, Ergonomics **20**, 121 (1977).
[40] National Ski Areas Association (NSAA), 17th International Congress on Ski Trauma and Skiing Safety (ISSS 2007); available at: [http://www.ski-injury.com/research/isss_2007]. Accessed December 7, 2010.
[41] J. E. Shealy, C. F. Ettlinger, and R. J. Johnson, J. ASTM Int. **2**(7), (2005).
[42] K.-U. Schmitt, P. Niemetz, and M. Muser, J. ASTM Int. **7**(6), (2010).
[43] National Ski Areas Association (NSAA), Technical data from Titlis Rotair; available at: [http://www.titlis.ch/upload/technische_daten_e.pdf]. Accessed July 25, 2011.
[44] H. Blunck, M. Kjærgaard, and T. Toftegaard, Pervasive Comput. **6696**, 350 (2011).
[45] [www.coenosense.com].
[46] M. Wirz, C. Strohrmann, R. Patscheider, F. Hilti, B. Gahr, F. Hess, D. Roggen, and G. Tröster, in *Proceedings of the First International Symposium on From Digital Footprints to Social and Community Intelligence* (ACM, New York, NY, USA, 2011), pp. 7–12.
[47] C. Gear, *Numerical Initial Value Problems in Ordinary Differential Equations* (Prentice Hall PTR, Upper Saddle River, NJ, 1971), p. 253.
[48] R. Sadus, *Molecular Simulation of Fluids: Theory, Algorithms and Object-Orientation* (Elsevier Science, Amsterdam, 2002).

[49] Federal Office for Topography swisstopo, National Ski Areas Association (NSAA), DOM; available at: [http://www.swisstopo.admin.ch/internet/swisstopo/en/home/products/height/dom_dtm-av.html]. Accessed July 26, 2011.

[50] H. Davson and E. Perkins, National Ski Areas Association (NSAA), Human eye; available at: [http://www.britannica.com/EBchecked/topic/1688997/human-eye]. Accessed November 4, 2011.

[51] F. Bowden, Proc. R. Soc. London A **217**, 462 (1953).

[52] M. Leino, E. Spring, and H. Suominen, Wear **86**, 101 (1983).

[53] P. Kaps, W. Nachbauer, and M. Mössner, Skiing Trauma Safety **10**, 165 (1996).

[54] L. Brownlie, G. Larose, A. D'Auteuil, T. Allinger, F. Meinert, P. Kristofic, S. Dugas, R. Boyd, and D. Stephens, Procedia Eng. **2**, 2375 (2010).